Article:
Zachariou, Nicholas orcid.org/0000-0001-7621-5612, Munevar, Edwin, Berman, Barry et al. (10 more authors) (2022) Beam-spin asymmetry $Σ$ for $Σ^-$ hyperon photoproduction off the neutron. Physics Letters B. 136985. ISSN 0370-2693

https://doi.org/10.1016/j.physletb.2022.136985

Beam-spin asymmetry Σ for Σ^- hyperon photoproduction off the neutron

N. Zachariou,[55,*] E. Munevar,[44] B.L. Berman,[15,†] P. Bydžovský,[31] A. Cieplý,[31] G. Feldman,[15] Y. Ilieva,[54] P. Nadel-Turonski,[8] D. Skoupil,[31] A.V. Sarantsev,[16] D. P. Watts,[55] M.J. Amaryan,[36] G. Angelini,[15] W.R. Armstrong,[1] H. Atac,[40] H. Avakian,[41] L. Barion,[18] M. Bashkanov,[55] M. Battaglieri,[41,20] I. Bedlinskiy,[30] F. Benmokhtar,[11] A. Bianconi,[47,23] L. Biondo,[20,17,49] A.S. Biselli,[12] M. Bondi,[20] F. Bossù,[7] S. Boiarinov,[41] W.J. Briscoe,[15] W.K. Brooks,[45,41] D. Bulumulla,[36] V.D. Burkert,[41] D.S. Carman,[41] J.C. Carvajal,[13] A. Celentano,[20] P. Chatagnon,[24] T. Chetry,[29] G. Ciullo,[18,46] L. Clark,[52] P.L. Cole,[28] M. Contalbrigo,[18] G. Costantini,[47,23] V. Crede,[14] A. D'Angelo,[21,50] N. Dashyan,[59] R. De Vita,[20] M. Defurne,[7] A. Deur,[41] S. Diehl,[37,43] C. Djalali,[35,54] R. Dupre,[24] M. Dugger,[2] H. Egiyan,[41,32] M. Ehrhart,[1] A. El Alaoui,[45] L. El Fassi,[29,1] P. Eugenio,[14] G. Fedotov,[39,‡] S. Fegan,[55] A. Filippi,[22] A. Fradi,[51] G. Gavalian,[41,36] G.P. Gilfoyle,[53] F.X. Girod,[41,7] C. Gleason,[42] A.A. Golubenko,[39] R.W. Gothe,[54] K.A. Griffioen,[58] M. Guidal,[24] K. Hafidi,[1] H. Hakobyan,[45,59] M. Hattawy,[36] T.B. Hayward,[43] D. Heddle,[9,41] K. Hicks,[35] A. Hobart,[24] M. Holtrop,[32] D.G. Ireland,[52] E.L. Isupov,[39] D. Jenkins,[56] H.S. Jo,[27,24] K. Joo,[43] D. Keller,[57] A. Khanal,[13] M. Khandaker,[34,§] A. Kim,[43] F.J. Klein,[6] A. Kripko,[37] V. Kubarovsky,[41,38] L. Lanza,[21] M. Leali,[47,23] K. Livingston,[52] I.J.D. MacGregor,[52] D. Marchand,[24] N. Markov,[41,43] L. Marsicano,[20] V. Mascagna,[48,23] B. McKinnon,[52] S. Migliorati,[47,23] T. Mineeva,[45] M. Mirazita,[19] V. Mokeev,[41,39] C. Munoz Camacho,[24] P. Nadel-Turonski,[41,6] K. Neupane,[54] S. Niccolai,[24] G. Niculescu,[26] T.R. O'Connell,[43] M. Osipenko,[20] A.I. Ostrovidov,[14] P. Pandey,[36] M. Paolone,[33] L.L. Pappalardo,[18,46] R. Paremuzyan,[41] E. Pasyuk,[41] W. Phelps,[9] O. Pogorelko,[30] J.W. Price,[3] Y. Prok,[36,57] B.A. Raue,[13] M. Ripani,[20] J. Ritman,[25] A. Rizzo,[21,50] G. Rosner,[52] J. Rowley,[35] F. Sabatie,[7] C. Salgado,[34] A. Schmidt,[15] R.A. Schumacher,[5] Y.G. Sharabian,[41] E.V. Shirokov,[39] U. Shrestha,[43] D. Sokhan,[52] O. Soto,[19] N. Sparveris,[40] S. Stepanyan,[41] P. Stoler,[43,38] I.I. Strakovsky,[15] S. Strauch,[54] R. Tyson,[52] M. Ungaro,[41,43] L. Venturelli,[47,23] H. Voskanyan,[59] A. Vossen,[10,41] E. Voutier,[24] K. Wei,[43] X. Wei,[41] R. Wishart,[52] M.H. Wood,[4,54] B. Yale,[58] J. Zhang,[57,36] and Z.W. Zhao[10,54]

(CLAS Collaboration)

[1] *Argonne National Laboratory, Argonne, Illinois 60439*
[2] *Arizona State University, Tempe, Arizona 85287-1504*
[3] *California State University, Dominguez Hills, Carson, California 90747*
[4] *Canisius College, Buffalo, NY*
[5] *Carnegie Mellon University, Pittsburgh, Pennsylvania 15213*
[6] *Catholic University of America, Washington, D.C. 20064*
[7] *IRFU, CEA, Université Paris-Saclay, F-91191 Gif-sur-Yvette, France*
[8] *CFNS Stony Brook University, Stony Brook, New York 11794*
[9] *Christopher Newport University, Newport News, Virginia 23606*
[10] *Duke University, Durham, North Carolina 27708-0305*
[11] *Duquesne University, 600 Forbes Avenue, Pittsburgh, Pennsylvania 15282*
[12] *Fairfield University, Fairfield, Connecticut 06824*
[13] *Florida International University, Miami, Florida 33199*
[14] *Florida State University, Tallahassee, Florida 32306*
[15] *The George Washington University, Washington, DC 20052*
[16] *Helmholtz-Institut fuer Strahlen- und Kernphysik, Universität Bonn, 53115 Bonn, Germany*
[17] *INFN, Sezione di Catania, 95123 Catania, Italy*
[18] *INFN, Sezione di Ferrara, 44100 Ferrara, Italy*
[19] *INFN, Laboratori Nazionali di Frascati, 00044 Frascati, Italy*
[20] *INFN, Sezione di Genova, 16146 Genova, Italy*
[21] *INFN, Sezione di Roma Tor Vergata, 00133 Rome, Italy*
[22] *INFN, Sezione di Torino, 10125 Torino, Italy*
[23] *INFN, Sezione di Pavia, 27100 Pavia, Italy*
[24] *Universit'e Paris-Saclay, CNRS/IN2P3, IJCLab, 91405 Orsay, France*
[25] *Institute fur Kernphysik (Juelich), Juelich, Germany*
[26] *James Madison University, Harrisonburg, Virginia 22807*
[27] *Kyungpook National University, Daegu 41566, Republic of Korea*
[28] *Lamar University, 4400 MLK Blvd, PO Box 10046, Beaumont, Texas 77710*
[29] *Mississippi State University, Mississippi State, MS 39762-5167*
[30] *National Research Centre Kurchatov Institute - ITEP, Moscow, 117259, Russia*
[31] *Nuclear Physics Institute of the Czech Academy of Sciences, 250 68 Řež, Czechia*
[32] *University of New Hampshire, Durham, New Hampshire 03824-3568*
[33] *New Mexico State University, PO Box 30001, Las Cruces, New Mexico 88003, USA*
[34] *Norfolk State University, Norfolk, Virginia 23504*
[35] *Ohio University, Athens, Ohio 45701*

[36] Old Dominion University, Norfolk, Virginia 23529
[37] II Physikalisches Institut der Universitaet Giessen, 35392 Giessen, Germany
[38] Rensselaer Polytechnic Institute, Troy, New York 12180-3590
[39] Skobeltsyn Institute of Nuclear Physics, Lomonosov Moscow State University, 119234 Moscow, Russia
[40] Temple University, Philadelphia, Pennsylvania 19122
[41] Thomas Jefferson National Accelerator Facility, Newport News, Virginia 23606
[42] Union College, Schenectady, New York, 12308
[43] University of Connecticut, Storrs, Connecticut 06269
[44] Universidad Distrital Francisco José de Caldas, Bogotá, Colombia
[45] Universidad Técnica Federico Santa María, Casilla 110-V Valparaíso, Chile
[46] Universita' di Ferrara , 44121 Ferrara, Italy
[47] Università degli Studi di Brescia, 25123 Brescia, Italy
[48] Università degli Studi dell'Insubria, 22100 Como, Italy
[49] Università degli Studi di Messina, 98166 Messina, Italy
[50] Università di Roma Tor Vergata, 00133 Rome, Italy
[51] University of Gabes, 6072-Gabes, Tunisia
[52] University of Glasgow, Glasgow G12 8QQ, United Kingdom
[53] University of Richmond, Richmond, Virginia 23173
[54] University of South Carolina, Columbia, South Carolina 29208
[55] University of York, York YO10 5DD, United Kingdom
[56] Virginia Tech, Blacksburg, Virginia 24061-0435
[57] University of Virginia, Charlottesville, Virginia 22901
[58] College of William and Mary, Williamsburg, Virginia 23187-8795
[59] Yerevan Physics Institute, 375036 Yerevan, Armenia

(Dated: July 7, 2021)

We report a new measurement of the beam-spin asymmetry $\mathbf{\Sigma}$ for the $\vec{\gamma}n \to K^+\Sigma^-$ reaction using quasi-free neutrons in a liquid-deuterium target. The new dataset includes data at previously unmeasured photon energy and angular ranges, thereby providing new constraints on partial wave analyses used to extract properties of the excited nucleon states. The experimental data were obtained using the CEBAF Large Acceptance Spectrometer (CLAS), housed in Hall B of the Thomas Jefferson National Accelerator Facility (JLab). The CLAS detector measured reaction products from a liquid-deuterium target produced by an energy-tagged, linearly polarised photon beam with energies in the range 1.1 to 2.3 GeV. Predictions from an isobar model indicate strong sensitivity to $N(1720)3/2^+$, $\Delta(1900)1/2^-$, and $N(1895)1/2^-$, with the latter being a state not considered in previous photoproduction analyses. When our data are incorporated in the fits of partial-wave analyses, one observes significant changes in γ-n couplings of the resonances which have small branching ratios to the πN channel.

1. INTRODUCTION

The excitation spectrum of the nucleon provides fundamental information on the dynamics and interactions of its constituents, the quarks and gluons, and is an important tool to achieve a more detailed understanding of the nature of Quantum Chromodynamics (QCD) in the non-perturbative regime. Phenomenological constituent quark models [1–6] and lattice QCD [7–9] predict a plethora of excited states of the nucleon that have yet to be experimentally determined. Alternative interpretations of nucleon structure that result in a reduced number of excited states (and therefore fewer "missing" resonances) have also been proposed [10–13]. Experimentally establishing the existence, or absence, of these missing nucleon resonances in nature has thus the potential to provide important insights into fundamental nucleon structure. As a result, the investigation continues to be a major focus at the world's leading electromagnetic beam facilities. Here we report a new precise measurement of the single polarisation observable, $\mathbf{\Sigma}$, and we discuss the effect this dataset has on partial wave analyses and models that aim at understanding the excited spectrum of nucleons.

The clean extraction of the nucleon excitation spectrum from experiment is complicated by the fact that the excited states are short-lived (broad) and overlapping. This complicates the extraction of their fundamental properties (photocouplings, lifetimes, spins, parities, decay branches, and even existence), with the difficulties exacerbated for states that produce weak signals in the decay channel under study. In the photoproduction of a pseudoscalar meson off the nucleon, the excited nucleon states contribute through their initial photoexcitation from the nucleon followed by the strong decay of the state. Values of the four complex amplitudes may be extracted up to an arbitrary phase, given data from a suitable combination of polarization measurements of suf-

* nicholas@jlab.org
† Deceased
‡ Current address:Ohio University, Athens, Ohio 45701
§ Current address:Idaho State University, Pocatello, Idaho 83209

ficient accuracy, which would therefore provide a maximum constraint on subsequent partial-wave analyses [14]. It has been recently argued that a reduced requirement on the number of measured observables may still allow convergence to a unique set of multipole amplitudes [15].

It is clear that eliminating the ambiguities in partial-wave analysis extraction of the excited nucleon states requires a precise and complete set of measurements of single- and double-polarisation observables, involving polarised beams, targets, and recoiling baryon polarimetry [14, 16–19]. Furthermore, measurements on both proton and (more challenging) neutron targets are indispensable, since resonances can have isospin dependent photocouplings [20, 21]. Additionally, the predicted differences in the preferred decay branches of individual states [2, 14, 22], mean that measurement of a wide range of pseudoscalar meson photoproduction final states, including $N\pi$, $K\Lambda$, $K\Sigma$ are crucial, and even data on vector meson (*e.g.,* $N\omega$) or multiple meson decays (*e.g.,* $N\pi\pi$) could be necessary. A recent review of the available results on non-strange baryon spectroscopy is given in Ref. [23].

The relative importance of decay channels to strange quark containing particles (*e.g.,* $K\Lambda$, $K\Sigma$) for missing or poorly established states has been emphasized by constituent quark model calculations [2]. Recent measurements of exclusive photoproduction of $K\Lambda$ and $K\Sigma$ from proton targets [24, 25] was key to achieve sensitivity to the newly discovered states reported in the PDG 2020 [26]. However, the corresponding data from neutron targets are much more limited. Although the differential cross section for $K^+\Sigma^-$ [27, 28] and $K^0\Lambda$ [28] reactions are measured with good precision, only one single polarisation measurement exists. The beam-spin asymmetry, $\mathbf{\Sigma}$, was originally obtained at LEPS [27], having kinematical coverage only at very forward kaon angles. The few double-polarisation measurements, for $K^+\Sigma^-$ [29], $K^0\Lambda$, and $K^0\Sigma^0$ [30], have more complete kinematic coverage but modest statistical accuracy, limiting definitive interpretations about contributing resonant states in partial wave analyses. It was highlighted in the most recent work on the beam-target helicity asymmetry in $K^+\Sigma^-$ photoproduction [29] that the $\mathbf{\Sigma}$ at backward kaon angles showed an enhanced sensitivity to the contribution of the $N(2120)3/2^-$ (D_{13}) excited state, which was found to improve the interpretation of the beam-target helicity asymmetry data [29].

In this work, we provide new experimental data on the beam-spin asymmetry $\mathbf{\Sigma}$ for the reaction $\vec{\gamma}n \to K^+\Sigma^-$, for the first time covering a wide range of kinematics and in previously unexplored mass ranges for contributing states. The experiment used a linearly-polarised tagged-photon beam incident on a (bound) quasi-free neutron target (liquid deuterium). The paper is ordered as follows: Sec. 2 provides a brief description of the experimental setup, Sec. 3 describes the method we employed to determine the observable $\mathbf{\Sigma}$, and details of the data analysis procedure and a description of the systematic uncertainties are discussed in Secs. 4 and 5, respectively. The results and a discussion of their implications are presented in Sec. 6.

2. EXPERIMENTAL SETUP

The data for this work were collected during the E06-103 experiment [31], which was conducted at the Thomas Jefferson National Accelerator Facility (JLab) utilising the Continuous Electron Beam Accelerator Facility (CEBAF) and the CEBAF Large Acceptance Spectrometer (CLAS) [32] housed in Hall B. The CLAS detector was comprised of a drift-chamber (DC) tracking system, a time-of-flight (ToF) system, and a calorimeter system that allowed particle identification and four-vector determination for charged and neutral particles. The charged particles' momenta were determined by tracing them as they traversed a toroidal magnetic field, providing momentum resolution of $\sigma_p/p \sim 1\%$. A start counter (ST) [33] that surrounded the target cell provided the event start-time information in photoproduction experiments. The ST, in conjunction with the ToF system, was used to determine the speed of charged particles. The E06-103 experiment utilised a 40-cm long liquid-deuterium target, centered 20 cm upstream of the nominal CLAS center to maximize acceptance for hyperon decays. Overall, the CLAS detector provided an efficient detection of charged particles over a large fraction of the full solid angle (between 8° and 142° in polar angles with ∼83% azimuthal coverage).

Hall B also housed the Tagger Facility [34], which enabled the selection and characterisation of the photons that initiated the photo-induced reactions detected within the CLAS detector on an event-by-event basis. The real photon beam was produced via the bremsstrahlung technique, by impinging a monochromatic electron beam on a thin radiator. The post-bremsstrahlung electrons were momentum analysed in a magnetic spectrometer that provided energy and timing information of the incident photon beam. With an energy resolution of ∼0.2%, this system permitted the tagging of photons with energies between 20% and 95% of the incident electron beam energy. The production of linearly polarized photons was based on the coherent bremsstrahlung radiation technique [35] utilising a 50-μm thick diamond radiator. With the use of a precise goniometer, data for two orientations of the photon polarisation were collected: one parallel (*Para*) and one perpendicular (*Perp*) to the Hall-B floor. Data were also obtained using an amorphous carbon radiator that enabled the determination of the degree of photon polarisation as discussed in the next section. For a fixed electron energy, the position of the coherent edge [1] was selected

[1] The coherent edge refers to the sharp falling edge in the enhancement spectrum as indicated in Fig. 1.

by appropriately orienting the diamond radiator. Data were obtained for different electron beam energies, varying from 3.3 to 5.2 GeV, to enhance the degree of photon polarisation in six coherent peak positions, in steps of 200 MeV between 1.1 and 2.3 GeV.

3. BEAM-SPIN ASYMMETRY

The differential cross section for meson photoproduction off an unpolarised target with a linearly polarised photon beam is given by [36]:

$$\frac{d\sigma}{d\Omega} = \left(\frac{d\sigma}{d\Omega}\right)_0 [1 - P_{lin}\mathbf{\Sigma}\cos(2\eta)], \quad (1)$$

where P_{lin} is the magnitude of the beam polarisation vector at an angle η to the reaction plane[2]. The above equation is obtained by integrating over the angular distribution of the hyperon decay products [3] ($\Sigma^- \to n\pi^-$ with a 99.85% branching ratio). The determination of $\mathbf{\Sigma}$ was done using a maximum likelihood approach. The likelihood function for a given event, i, taken from the cross-section Eq. (1) is

$$L_i = c\left[1 - P^i_{lin}\mathbf{\Sigma}\cos(2\eta_i)\right] A, \quad (2)$$

where c is a normalisation coefficient and A is the detector acceptance. In the construction of the log-likelihood function an approximation was made concerning the detector acceptance. Specifically, an acceptance that is largely independent of the kinematic variable η was assumed, which resulted in a normalisation coefficient that is independent of the value of the polarisation observable. This approximation significantly simplified the extraction of the observable, but could potentially result in systematic biases. Extensive studies of such systematic effects showed that any residual effects on the polarisation observable are negligible.

The log-likelihood function that was maximized to obtain the polarisation observables is thus given by

$$\log L = b + \sum_i \log\left[1 - P^i_{lin}\mathbf{\Sigma}\cos(2\eta_i)\right], \quad (3)$$

where the constant b is the observable-independent constant that absorbs the normalisation coefficient (associated with the photon flux) and the detector acceptance. The summation is over all events within a given kinematic bin. A transformation from the reaction frame (where the y axis is perpendicular to the reaction plane) to the lab frame (where the y axis is vertical to the Hall B floor) was done using the following equations for the two orthogonal orientations of the photon polarisation (*Para* and *Perp*)

$$\eta^{Para} = -(\phi - \phi_0)$$
$$\eta^{Perp} = \frac{\pi}{2} - (\phi - \phi_0),$$

where ϕ is the meson azimuthal angle as measured in the lab frame, and ϕ_0 is the offset of the photon polarisation with respect to the lab x (for *Para*) or y (for *Perp*) axis. Using the above two equations, Eq. (3) can be written as

$$\log L = b + \sum_i \log\left[1 - \mathbb{P}^i_{lin}\mathbf{\Sigma}\cos(2\phi_i - 2\phi_0)\right], \quad (4)$$

where $\mathbb{P}^i_{lin} = P^i_{lin}$ for *Para* events, and $\mathbb{P}^i_{lin} = -P^i_{lin}$ for *Perp* events[4]. This likelihood function was maximized using MINUIT [37] to obtain the value of the observable $\mathbf{\Sigma}$ and its uncertainty. The ϕ_0 offset was determined using a high-statistics channel from the same dataset (single pion photoproduction), found to be consistent with zero.

The determination of the beam-spin asymmetry requires a precise knowledge of the degree of photon polarisation, P^i_{lin}. The determination of P^i_{lin} involved using the coherent and incoherent bremsstrahlung spectra to obtain an enhancement distribution that was then fit by a spectrum obtained from theoretical bremsstrahlung calculations (referred to as the Analytical Bremsstrahlung Calculation – ANB). Specifically, the enhancement distribution was obtained by taking the ratio of the photon energy spectrum from the diamond radiator to one obtained using the amorphous radiator, and was used to constrain the relative contribution of the coherent and incoherent bremsstrahlung to the total photon yield. This ratio also removed Tagger channel efficiency fluctuations allowing a precise determination of the degree of photon polarisation. Subsequently, the enhancement plot was fit with the theoretical spectrum from ANB. More details on the procedure can be found in Refs. [35, 38, 39].

The ANB calculation takes into account 17 experimental parameters characterizing the geometry of the radiator, collimator, and photon beam. Several of these parameters were measured experimentally (such as the photon beam energy and beam spot size), whereas others (such as electron beam divergence on the radiator) were varied until a good agreement was obtained between the enhancement plot and the ANB calculation. These parameters were then used to calculate the degree of polarisation as a function of photon energy. An example of a fit to an enhancement spectrum with the ANB calculation is shown in Fig. 1 along with the calculated photon

[2] The reaction plane is defined by the cross product of the incoming photon and the outgoing meson.

[3] The full cross section equation as shown in Ref. [36] depends on additional double polarisation observables accessible by studying the angular dependence of the hyperon decay products. Integrating over the nucleon angle in the hyperon rest frame would eliminate such contributions only when the detector acceptance is uniform in these kinematics. In principle, the detector acceptance might affect the implied integration over the angles of the hyperon decay products. However, as the self-analyticity of the Σ^- is very small ($\alpha = 0.068$), any double polarisation observables contributions/effects to the beam-spin asymmetry are negligible compared to the quoted systematics.

[4] The sign of $\mathbb{P}_\gamma$ absorbs the sign from the trigonometric function when translating η to ϕ, since $\cos(180 - 2\phi) = -\cos(2\phi)$.

polarisation (dashed line). This procedure was done for the various coherent-edge positions, allowing the determination of the photon polarisation on an event-by-event basis. The degree of photon polarisation throughout the experiment was on average 72%.

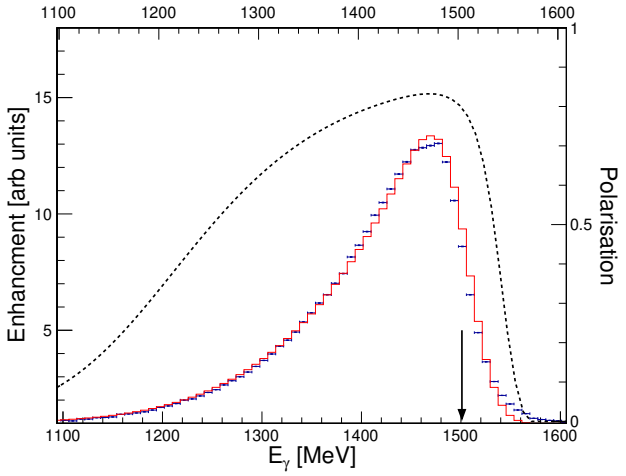

FIG. 1. Example of an enhancement distribution (blue points) fit with the ANB calculation (red histogram) to determine the photon polarisation (dashed line). The arrow indicates the coherent edge position.

4. DATA ANALYSIS

The reaction of interest was reconstructed by selecting events with exactly one negative pion and one positive kaon, identifying the photon that initiated it, and applying the missing-mass technique under the assumption that the target was a nucleon at rest. Particle identification was done by following the standard procedures adopted for E06-103 analyses, by comparing the particle's speed calculated from two independent measurements: time-of-flight and momentum, with the latter requiring an assumption about the particle's rest mass. The photon that initiated the reaction detected in CLAS was identified by timing coincidence at the event vertex between the tracks in CLAS and photons, with the latter being reconstructed using information from the Tagger spectrometer. The 2-ns beam bunch structure of the delivered electron beam allowed an unambiguous identification of the photon that initiated the reaction for $\sim 90\%$ of the events. The remaining 10% of events were associated with two or more photons with coincidence times within ± 1 ns, and such events were discarded from further analysis.

A fraction of positive pions from the reactions $\gamma N \to \pi^+\pi^- X$ (where N can be either a proton or a neutron) were misidentified as kaons. Contributions from these events were eliminated by applying a cut on the mass of the missing state X in $\gamma N \to \pi^+\pi^- X$ (assuming the reconstructed kaon was a misidentified pion).

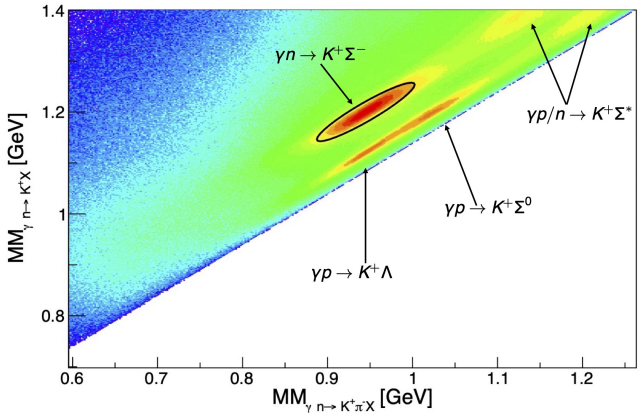

FIG. 2. Mass of the missing state X of $\gamma n \to K^+ X$ vs. $\gamma n \to K^+\pi^- X$ indicating the different physics channels that contribute to the event sample.

The reaction of interest was identified by further exploiting the missing-mass technique. Specifically, the correlation in the missing mass, m_X, distribution of $\gamma n \to K^+ X$ ($MM_{\gamma n\to K^+X}$) and the m_X distribution of $\gamma n \to K^+\pi^- X$ ($MM_{\gamma n\to K^+\pi^-X}$) allows a clean identification of the reaction of interest. This correlation is shown Fig. 2 along with the elliptical (two-dimensional) cut employed to select the events of interest. The parameters of the elliptical cut were optimised using simulated data (processed through a realistic detector simulation). This approach resulted in an event sample where background contributions were minimised, while retaining a large fraction of good events. With the parameters of the adopted cut, the average background contributions were found to be below 2% (with such contributions accounted for in the systematic uncertainty, as listed in Table I).

5. SYSTEMATIC UNCERTAINTIES

An extensive investigation of potential sources of systematic uncertainty was carried out with estimates summarised in Table I. Most sources have negligible contributions compared to the statistical uncertainty of the data. The largest contribution originates from uncertainties of the degree of photon polarisation, and the second largest is due to the dilution of the measured observable stemming from having a bound rather than a free neutron target. The latter arises from effects of the Fermi motion of the target neutron and Final State Interactions (FSI) of the outgoing reaction products with the deuterium remnants. Such dilution effects were investigated in detail using a smaller subset of the data sample in which the final-state neutron was detected in addition to the K^+ and π^- [40], as well as through simulations. Only a weak dependence of $\mathbf{\Sigma}$ on the momentum of the target neutron was discovered. The asymmetric (positive) systematic uncertainties reflect the fact that FSI effects

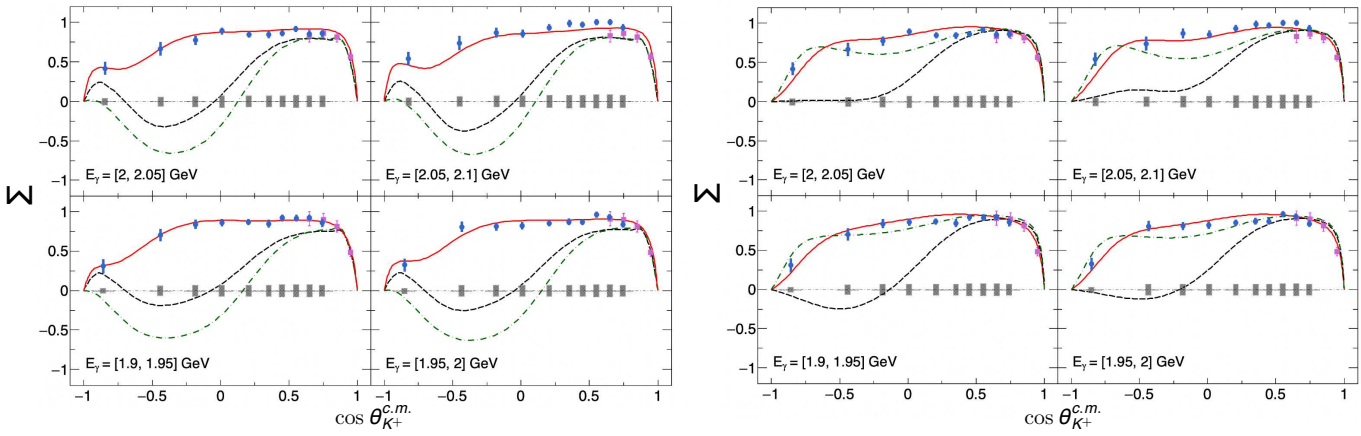

FIG. 3. Beam spin asymmetry $\boldsymbol{\Sigma}$ as a function of kaon angle in the *c.m.* for four photon energy bins as indicated in the panels. Experimental data from this work are shown with solid blue circles, whereas magenta points show the previously published results from LEPS [27]. Statistical uncertainties are indicated with the errors bars, whereas the total systematic uncertainties of the CLAS results are shown by the shaded bar chart. The left set of panels shows the new Bonn-Gatchina solution that was fit to our data (red solid lines), as well as previously published Bonn Gatchina solutions with (green dash dotted lines) and without (black dashed lines) contributions from the D_{13} resonance (see Ref. [29] for a detailed discussion). The right set of panels show the full solution of the isobar model (red solid lines), as well as the solution without the $N(1720)\,3/2^+$ (black dashed lines), and the $\Delta(1900)\,1/2^-$ (green dashed dotted lines) resonance.

only dilute and do not enhance the measured $\boldsymbol{\Sigma}$. Additional sources, including background contributions and misidentified kaon events, contributed to a much smaller degree as summarised in Table I. The uncertainties are split in two categories: an absolute uncertainty that is the same for all kinematics, and a relative uncertainty (associated with the photon polarisation) with its magnitude determined for each point.

Source	σ^{sys}
Maximum Likelihood	negligible
Kaon PID	± 0.008
Pion PID	± 0.004
Photon selection	± 0.002
Misidentified kaons	± 0.003
Kaon Decay in flight	± 0.0064
Σ^* background contribution	± 0.007
Λ and Σ^0 contributions	± 0.008
Fiducial cut	± 0.002
FSI	$+0.024$
Total Absolute Systematic	$^{+0.029}_{-0.016}$
Photon polarisation	**8%**

TABLE I. Summary of systematic uncertainties of $\boldsymbol{\Sigma}$.

6. RESULTS AND DISCUSSION

The extracted $\boldsymbol{\Sigma}$ data are shown by the blue solid circles in Figs. 3 and 4, binned in 50-MeV wide photon-energy bins (from 1.1 to 2.3 GeV) and in 10 bins of kaon production angle in the center-of-momentum (*c.m.*) frame[5], $\cos\theta_{K^+}$. Figure 3 shows how the new precise results in four photon-energy bins compare with previous and current Bonn Gatchina solutions (left) or with an isobar model predictions that focuses on contributions from specific resonance states (right). Figure 4 compares the two new solutions for all available kinematic bins as discussed in detailed later on. The angular bins are contiguous but with varying widths to accommodate the angular variation of the reaction yield as to keep the statistics per bin rather constant. The statistical uncertainties are shown by the error bars for each point, and the systematic uncertainties are shown by the grey bands. For all photon energies, the measured $\boldsymbol{\Sigma}$ is large, positive, and for forward-central kaon angles rather uniform. The data exhibit a fall off at backward kaon angles, with $\boldsymbol{\Sigma}$ typically larger in the forward angle region. As $\boldsymbol{\Sigma}$ must have a value of 0 at $\cos\theta_{K^+} = \pm 1$, the observable values outside of our acceptance range (*i.e.,* between $\cos\theta_{K^+} = 0.75$ and $\cos\theta_{K^+} = 1.0$ for forward angles) must vary rapidly to reach 0. At backward angles the transition to zero exhibits a more gradual trend.

The published results for $\boldsymbol{\Sigma}$ from LEPS [27] are also shown by the magenta solid squares in Figs. 3 and 4. The LEPS data are limited to very forward kaon angles and have larger statistical and systematic uncertainties than our data. Nevertheless, the results from CLAS are in good agreement with these previously published data (note the LEPS data were obtained in 100-MeV wide photon energy bins). The improvement in the quality and range of available data with this new measurement

[5] Commonly known as the center-of-mass frame.

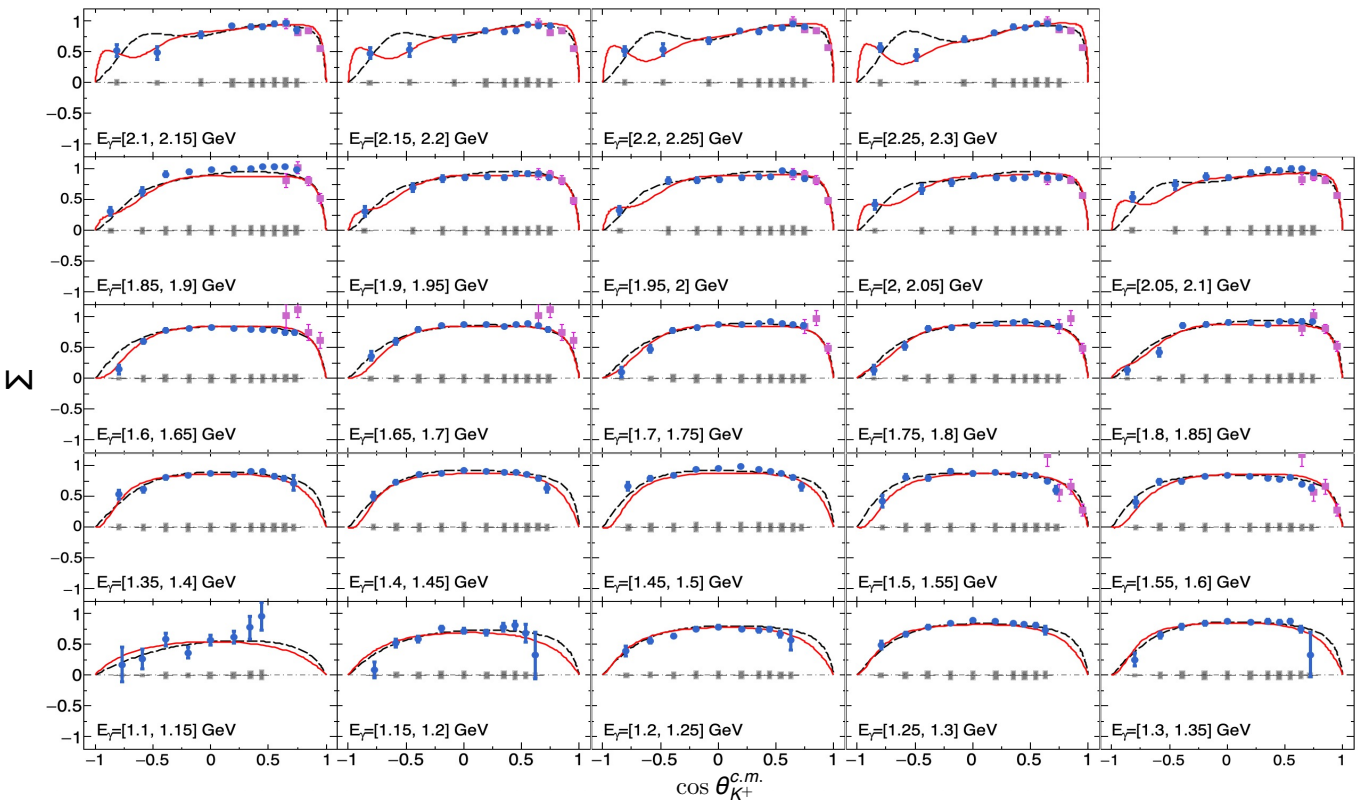

FIG. 4. Beam spin asymmetry $\mathbf{\Sigma}$ as a function of kaon angle in the *c.m.* The different panels show bins in photon energy. Experimental data from this work are shown with solid blue circles, whereas magenta points show the previously published results from LEPS [27]. Statistical uncertainties are indicated with the errors bars, whereas the total systematic uncertainties of the CLAS results are shown by the shaded bar chart. The black dashed line indicates the full solution of the isobar model as described in the text and the red solid line indicates the new Bonn-Gatchina solution that was fit to our data.

is apparent in Fig. 4.

The solutions of the Bonn-Gatchina group BG2016 [41] (not shown here) predicted the beam asymmetry for the $\gamma n \to K^+\Sigma^-$ reaction above 1850 MeV to be negative at the backward and the central angular region. The most recent predictions from the Bonn-Gatchina model [29] with (without) the proposed D_{13} resonance are shown by the dash-dotted green (dashed black) lines in the left panels of Fig. 3 (only four representative photon energy bins are shown). These predictions were fit to the current world dataset in meson photoproduction, including the unpolarised differential cross section, the data on the beam-target helicity asymmetry measured by the CLAS Collaboration, and the LEPS data on the beam asymmetry, but excluding data from this work. The $\mathbf{\Sigma}$ data from LEPS were measured only in the very forward angular region and mostly were defined by the contribution from the t-channel exchange amplitudes. Moreover, the CLAS data on the unpolarized cross section and beam-target helicity asymmetry did not cover the very backward angular region, which allowed ambiguous solutions. It is clear that neither of these solutions can reproduce the angular dependence of $\mathbf{\Sigma}$, with discrepancies especially apparent at photon energies above 1.3 GeV. Clearly, the new data have the potential to impact this partial-wave analysis and, therefore, the excited nucleon spectrum therein.

The inclusion of the new beam asymmetry data in the full combined analysis led to significant changes in the γ-n couplings of the resonances that have small branching ratios to the πN channel. The largest changes were found in the D_{13} and P_{13} partial waves: here the states in the region above 1850 MeV were mostly seen in the reactions with open strangeness. The newly obtained solution is indicated by the red solid curves in Figs. 3 and 4. The detailed and systematic analysis of this solution will be presented in a separate paper, which will follow the present publication.

The full predictions from an isobar model [42] for $\mathbf{\Sigma}$ are shown by the black dashed line in Fig. 4. These are based on an effective Lagrangian in a tree-level approximation. The non-resonant part of the amplitude consists of the Born terms and exchanges of resonances in the t- (K^* and K_1) and u-channels (Σ^*). The main coupling constant $g_{K^+\Sigma^-n} = \sqrt{2}g_{K^+\Sigma^0p} = 1.568$, which determines the strength of the Born terms, was taken from the $K^+\Lambda$ channel [42] and kept unchanged in the present fit. The resonant part is modeled by s-channel exchanges of nu-

cleon and Δ resonances with masses below about 2 GeV. Hadronic form factors included in the strong vertices account for hadron structure and regularize the amplitude at large energies. The form factors are introduced in the way that keeps gauge invariance intact, in analogy with the method used in Refs. [42] and [43]. The solution presented in Fig. 4 was fit to the current CLAS (and LEPS) $\mathbf{\Sigma}$ data, as well as the differential cross section of $\gamma n \to K^+\Sigma^-$ from CLAS [28]. In total, 24 free parameters (22 couplings and 2 hadron form factor cut-offs) were used to fit 332 cross section data points and 284 asymmetries, all of them are restricted to energies up to $E_\gamma = 2.6$ GeV. The fit parameters of the isobar model were extracted adopting the procedure outlined in Refs. [42, 43] for the $K^+\Lambda$ channel. More details are provided in Ref. [44].

The considered set of nucleon resonances in the isobar model was motivated by previous analyses of $K^+\Lambda$ [42, 43] and $K\Sigma$ photoproduction [45]. Some additional N^* resonances predicted to strongly couple the $K\Sigma$ channel were also investigated in the analysis. The variant with the smallest χ^2/ndf and reasonable values of the parameters was selected. The complete set of resonances from this best fit is provided in Table II [6]. The solution indicates contribution from two kaon resonances, multiple nucleon resonances, one Δ resonance, and no hyperon resonances [7]. The combined asymmetry and cross section data show a strong sensitivity to $N(1720)\,3/2^+$, whose omission significantly diminishes both observables (see right panels of Fig. 3). Sensitivity was also observed from the $\Delta(1900)1/2^-$ resonance, specifically at central angles, as indicated by the green dashed dotted lines in the right panels of Fig. 3. A significant contribution of the $N(1895)\ 1/2^-$ state was obtained, a state not considered in previous photoproduction analyses, but with a relatively large $K\Sigma$ branching ratio. The role of hyperon resonances appears small, giving negligible effects on the predicted observables.

TABLE II. Characteristics of included resonances with their masses and widths taken as the PDG Breit-Wigner averages. The available branching ratios to the $K\Lambda$ and $K\Sigma$ channels are also taken from the PDG [26]. For the nucleon and Delta resonances, the values g_1 and g_2 show the baryon-$K\Sigma$ scalar and tensor couplings obtained in our fit, while for the K^* and K_1 states they represent the vector and tensor couplings, respectively.

Resonance	Mass	Width	Branching ratios		Couplings	
	(MeV)	(MeV)	ΛK	ΣK	g_1	g_2
$N(1535)\ 1/2^-$	1530	150	—	—	-0.709	—
$N(1650)\ 1/2^-$	1650	125	0.07	0.00	0.314	—
$N(1675)\ 5/2^-$	1675	145	—	—	-0.013	0.022
$N(1710)\ 1/2^+$	1710	140	0.15	0.01	-0.940	—
$N(1720)\ 3/2^+$	1720	250	0.05	0.00	-0.098	-0.082
$N(1875)\ 3/2^-$	1875	200	0.01	0.01	-0.220	-0.223
$N(1880)\ 1/2^+$	1880	300	0.16	0.14	-0.050	—
$N(1895)\ 1/2^-$	1895	120	0.18	0.13	-0.063	—
$N(1900)\ 3/2^+$	1920	200	0.11	0.05	-0.051	-0.004
$N(2060)\ 5/2^-$	2100	400	0.01	0.03	-0.00001	0.003
$N(2120)\ 3/2^-$	2120	300	—	—	-0.034	-0.010
$\Delta(1900)\ 1/2^-$	1860	250	—	0.01	0.298	—
$K^*(892)$	891.7	50.8	—	—	0.366	1.103
$K_1(1270)$	1270	90	—	—	-1.448	0.473

7. SUMMARY

We present the first precise measurement of the beam-spin asymmetry $\mathbf{\Sigma}$, employing a linearly polarised photon beam, for $\vec{\gamma}n \to K^+\Sigma^-$ up to photon energies of $E_\gamma = 2.3$ GeV. The new data obtained using a deuterium target agree well with previously published data from LEPS (limited only to forward angles), while significantly extending the available kinematic coverage for $\vec{\gamma}n \to K^+\Sigma^-$ down to photon energies of $E_\gamma = 1.1$ GeV and cover a large angular range. The new $\mathbf{\Sigma}$ data are an important addition to the world database and have a large effect on the determined γ-n couplings of resonances that have small branching ratios to the πN channels. The largest changes were found in the D_{13} and P_{13} partial waves. A more detailed analysis in the Bonn-Gatchina framework will be presented in a planned joint publication. The new data were also fit using an isobar model based on an effective Lagrangian in a tree-level approximation, with results indicating contributions from two kaon resonances, multiple nucleon resonances (with significant contributions from the $N(1720)3/2^+$ and $N(1895)1/2^-$), one Δ resonance, and no hyperon resonances. Details on the isobar model will also be presented in a longer planned joint publication.

8. ACKNOWLEDGMENTS

This work has been supported by the U.K. Science and Technology Facilities Council (ST/P004385/2, ST/T002077/1, and ST/L00478X/2) grants, as well as by the Czech Science Foundation GACR grant 19-19640S. We also acknowledge the outstanding efforts of the staff of the Accelerator and Physics Divisions at Jefferson

[6] Note that only the statistical uncertainties of the fit data were used in the computation of the χ^2, which results in a relatively large value $\chi^2/ndf = 2.39$ for the selected solution. This approach was chosen due to missing systematic uncertainties in some data sets. When systematics are taken into account, the χ^2 value typically drops without changing the quality of results.

[7] The obtained couplings g_1 and g_2 from the fit listed in Table II are all reasonable, as are the hadronic form factor cut-offs $\Lambda_{\rm bgr} = 0.874$ GeV and $\Lambda_N = 1.451$ GeV (see Ref. [43] for a description of these parameters).

Lab that made this experiment possible. The Southeastern Universities Research Association (SURA) operated the Thomas Jefferson National Accelerator Facility for the United States Department of Energy under contract DE-AC05-06OR23177. Further support was provided by the National Science Foundation, the Italian Istituto Nazionale di Fisica Nucleare, the Chilean Comisión Nacional de Investigación Científica y Tecnológica (CONICYT), the French Centre National de la Recherche Scientifique, the French Commissariat à l'Energie Atomique, and the National Research Foundation of Korea.

[1] S. Capstick and W. Roberts, Prog. Part. Nucl. Phys. **45**, 241 (2000).
[2] S. Capstick and W. Roberts, Phys. Rev. D **58**, 074011 (1998).
[3] S. Capstick and N. Isgur, Phys. Rev. D **34**, 2809 (1986).
[4] U. Löring, B.Ch. Metsch, and H.R. Petry, Eur. Phys. J. A **10**, 395 (2001).
[5] L. Ya. Glozman, W. Plessas, K. Varga, and R. F. Wagenbrunn, Phys. Rev. D **58**, 094030 (1998).
[6] M. M. Giannini, E. Santopinto, and A. Vassallo, Eur. Phys. J. A **12**, 447 (2001).
[7] R. G. Edwards, J. J. Dudek, D. G. Richards, and S. J. Wallace, Phys. Rev. D **84**, 074508 (2011).
[8] J. J. Dudek and R.G. Edwards, Phys. Rev. D **85**, 054016 (2012).
[9] R. G. Edwards, N. Mathur, D. G. Richards, and S. J. Wallace, Phys. Rev. D **87**, 054506 (2013).
[10] M. Anselmino, E. Predazzi, S. Ekelin, S. Fredriksson, and D. B. Lichtenberg, Rev. Mod. Phys. **65**, 1199 (1993).
[11] S. J. Brodsky, Eur. Phys. J. A **31**, 638 (2007).
[12] E. E. Kolomeitsev and M. F. M. Lutz, Phys. Lett. B **585**, 243 (2004).
[13] S. S. Afonin, Int. J. Mod. Phys. A **22**, 4537 (2007).
[14] W-T. Chiang and F. Tabakin, Phys. Rev. C **55**, 2054 (1997).
[15] R. L. Workman, L. Tiator, Y. Wunderlich, M. Döring, and H. Haberzettl, Phys. Rev. C **95**, 015206 (2017).
[16] J. Nys, J. Ryckebusch, D. G. Ireland, and D. I. Glazier, Phys. Lett. B **759**, 260 (2016).
[17] A. M. Sandorfi, S. Hoblit, H. Kamano, and T. S. H. Lee, J. Phys. G **38**, 053001 (2011).
[18] C. G. Fasano, F. Tabakin, and B. Saghai, Phys. Rev. C **46**, 2430 (1992).
[19] G. Keaton and R. Workman, Phys. Rev. C **54**, 1437 (1996).
[20] A. M. Sandorfi and S. Hoblit, Nucl. Phys. A **914**, 538 (2013).
[21] T. Mart, C. Bennhold, and C. E. Hyde-Wright, Phys. Rev. C **51**, 1074(R) (1995).
[22] S. Capstick and W. Roberts, Phys. Rev. D **57**, 4301 (1998).
[23] D. G. Ireland, E. Pasyuk, and I. Strakovsky, Prog. Part. Nucl. Phys. **111**, 103752 (2020).
[24] A. V. Anisovich *et al.*, Phys. Rev. Lett. **119**, 062004 (2017).
[25] C. A. Paterson *et al.* (CLAS Collaboration), Phys. Rev. C **93**, 065201 (2016).
[26] P.A. Zyla *et al.* (Particle Data Group), Progress of Theoretical and Experimental Physics **2020**, 083C01 (2020).
[27] H. Kohri *et al.* (LEPS Collaboration), Phys. Rev. Lett. **97**, 082003 (2006).
[28] S. A. Pereira *et al.* (CLAS Collaboration), Phys. Lett. B **688**, 289 (2010).
[29] N. Zachariou *et al.* (CLAS Collaboration), Phys. Lett. B **808**, 135662 (2020).
[30] D. Ho *et al.* (CLAS Collaboration), Phys. Rev. C **98**, 045205 (2018).
[31] P. Nadel-Turonski *et al.*, Thomas Jefferson Lab, CLAS Approved Experiment **E06-103** (2006), `https://www.jlab.org/exp_prog/proposals/06/PR-06-103.pdf`.
[32] B. A. Mecking *et al.*, Nucl. Instrum. Meth. A **503**, 513 (2003).
[33] Y. G. Sharabian *et al.*, Nucl. Instrum. Meth. A **556**, 246 (2006).
[34] D. I. Sober *et al.*, Nucl. Instrum. Meth. A **440**, 263 (2000).
[35] H. Überall, Zeitschrift für Naturforschung A **17**, 332 (1962).
[36] I. S. Barker and A. Donnachie, Nucl. Phys. B **95**, 347 (1975).
[37] F. James and M. Winkler, "MINUIT User's Guide," (2004).
[38] K. Livingston, Jefferson Laboratory, CLAS Note **2011-020** (2011), `https://misportal.jlab.org/ul/Physics/Hall-B/clas/viewFile.cfm/2011-020.pdf?documentId=656`.
[39] N. Zachariou, Ph.D. Thesis George Washington University (2012), `http://www.jlab.org/Hall-B/general/thesis/Zachariou_thesis.pdf`.
[40] E. Munevar, Ph.D. Thesis George Washington University (2014), `https://www.jlab.org/Hall-B/general/thesis/Munevar_thesis.pdf`.
[41] J. Müller *et al.*, Phys. Lett. B **803**, 135323 (2020).
[42] D. Skoupil and P. Bydžovský, Phys. Rev. C **93**, 025204 (2016).
[43] D. Skoupil and P. Bydžovský, Phys. Rev. C **97**, 025202 (2018).
[44] P. Bydžovský, A. Cieplý, D. Petrellis, and D. Skoupil, prepared for publication (2021).
[45] J. C. David, C. Fayard, G. H. Lamot, and B. Saghai, Phys. Rev. C **53**, 2613 (1996).